Pure Appl. Geophys.

DOI 10.1007/s00024-016-1391-z

Pure and Applied Geophysics

Uppermost Inner Core Heterogeneity from Differential Travel Times of PKIKP vs. PKP-Bdiff and PKP-Cdiff Phases

Marian Ivan[1,2] and Xiaobo He[3]

Abstract—We evaluate the average P-wave velocity perturbations of the Earth's uppermost inner core (IC) by analyzing two pairs of core phases: PKIKP–PKP-Bdiff (456 observations in the distance range of 138.5°–142°) and PKIKP–PKP-Cdiff (1215 observations at 155°–162°). The former is most sensitive to inner core velocities in the depth range of 350–590 km and the latter from 0 to 100 km below the inner core boundary. The differential travel-time residuals exhibit the roughly "east–west" hemispheric pattern especially beneath the Pacific Ocean. Here, the separation between the two quasi-hemispheres is near the 150°W meridian (from PKP-Bdiff observations), but possibly rotated toward a NW–SE orientation, from PKP-Cdiff. Alternately, a velocity heterogeneity could be present here, in agreement with the previously reported PKIKP vs. PKP_{BC} observations. Assuming the conventional definition for the IC quasi-hemispheres (i.e., the QEH between 0° and 180°E, and the QWH between 0° and 180°W), the quasi-Eastern hemisphere exhibits perturbations of (+1.17 ± 0.04) % (from PKIKP–PKP-Bdiff) and (+0.19 ± 0.01) % (from PKIKP–PKP-Cdiff). The corresponding perturbations in the quasi-Western hemisphere are of (−0.06 ± 0.06) % and (−0.19 ± 0.02) %, respectively. An anomalous IC zone beneath the Indian Ocean is not conspicuous in our PKIKP–PKP-Cdiff observations. Beneath the North Atlantic, the separation between the IC quasi-hemispheres appears to be located between 60°W and 30°W from the PKP-Bdiff observations, but it remains unresolved from the PKP-Cdiff data, due to scarce observations here.

Key words: Uppermost inner core, diffracted PKP phases, PKIKP, inner core heterogeneity.

1. Introduction

The inner core (IC) has a major importance in understanding the various complex processes affecting the Earth, like the global dynamics and thermal evolution or stability of the geomagnetic dynamo (e.g., Deuss 2014; Tkalčić 2015). At a large scale, a variety of seismological studies indicated an apparent hemispherical pattern related to both anisotropy and heterogeneity of the uppermost IC (Tanaka and Hamaguchi 1997; Creager 1999; Niu and Wen 2001). The accurate geographical delimitation between the two IC quasi-hemispheres, the sharp or smooth nature of this transition, or the coupling/decoupling between the uppermost IC (UIC) and the F region (lowermost outer core, LOC) are, however, still questions of debate. For example, the boundary between the IC hemispheres in the North Pacific is estimated at a variety of values, i.e., close to 180°E, near 160°E, near 120°W, or near 151°W meridians (see a synopsis in Yee et al. 2014).

Regional or fine-scale velocity structures in the UIC have been reported by various studies, with the possible presence of a mushy zone, or a mosaic-like boundary between IC and the outer core (OC) (e.g., Loper and Roberts 1981; Krasnoshchekov et al. 2005). While with respect to a spherically symmetric Earth model, a positive velocity perturbation in the quasi-eastern hemisphere (QEH) and a negative perturbation in the quasi-western hemisphere (QWH) is unanimously accepted, whereas the amplitude of these perturbations and the corresponding global reference model are still debated subjects (e.g., Souriau et al. 2003; Tanaka 2012; Yee et al. 2014).

Base on the differential times and amplitudes of PKIKP vs. PKiKP recorded in the distance range of 135°–142°, a lopsided growth of Earth's IC has been proposed by Monnereau et al. (2010) to predict a hemispherical separation along 10°E and 170°W meridians, with smooth transitions between the two hemispheres (see also Alboussière et al. 2010). It is

[1] University of Bucharest, Bucharest, Romania. E-mail: marian.ivan@g.unibuc.ro
[2] National Institute for Earth Physics, Bucharest, Romania.
[3] Department of Marine Sciences, Zhejiang University, Hangzhou, China.

Published online: 06 September 2016

worth noting that some departures from a simple IC have been emerging recently. In particular, using core phases whose ray paths run beneath Antarctica, Ohtaki et al. (2012) concluded that the inner core does not have a simple hemispherical wave velocity pattern. Iritani et al. (2014) reported intricate heterogeneous structures at the top of the IC. Krasnoshchekov et al. (2016) outlined the presence of an anisotropic block in the IC beneath Southeastern Asia.

The majority of the seismological constraints regarding wave velocity perturbations and attenuation in the IC comes from the observations of travel time or frequency content of PKIKP (P wave transmitted through the IC) vs. PKP_{BC} (P wave bottoming in the lower OC) phases in the distance range of 148°–155°, sampling the IC in the depth range of 150–350 km below IC boundary. To a small extent, such studies also incorporated PKP-Cdiff data, at distances exceeding 154°–155° (e.g., Tanaka and Hamaguchi 1997; Creager 1999; Ohtaki et al. 2012; Cormier and Attanayake 2013), or to estimate the depth extent of the hemispherical inner core along equatorial paths (Tanaka 2012). PKP-Bdiff has been used to help with the interpretation of PKiKP vs. PKIKP differential times (Luo et al. 2002), or in relation to PKiKP (Yu and Wen 2006). In addition, a variety of other seismological approaches, such as PKIKP vs. PKP_{AB} (P wave bottoming in the upper OC) (e.g., Irving and Deuss 2011), absolute arrival times of PKIKP (Sun and Song 2002), and normal modes (e.g., Deuss et al. 2010), have been employed to investigate the core structure.

In this study, a large set of PKP-Bdiff (a diffracted P wave transmitted through the middle portion of the OC) (e.g., Wen and Helmberger 1998; Yu and Wen 2006) and PKP-Cdiff (P wave diffracting around the IC boundary) data is collected. As a result of a low-velocity zone of the liquid outer core, PKP-Bdiff phase is not predicted by ray theory, but it can be accurately synthesized by normal modes summation. PKP-Bdiff is turning within the middle of the OC, observed as a long-period wave at epicentral distances closer than the B—caustic point (located around 145°). It has an apparent slowness around 3.8 s/°, a value quite different from the PKIKP slowness (the last one being around 1.8 s/°). PKP-Cdiff phase is observed at distances larger than 155° (which corresponds to C—cut off point). To reproduce the two diffracted waves, the normal modes summation (Wang 1999) is employed to calculate the differential travel-time residuals. The travel-time perturbations due to the heterogeneities from the crust and mantle are further evaluated based on the LLNL-Earth 3D global velocity model (Simmons et al. 2012).

2. *Data Analysis and Results*

We collected a large number of conspicuous broad-band velocity PKP diffracted core phases recorded between 1989 and 2015 mainly in Europe and Asia (China and Japan) by various permanent and temporary networks, selecting 456 broad-band PKP-Bdiff recordings and 1215 broad-band PKP-Cdiff recordings, from a total of 71 events (see event parameters in Table 1).

At distances less than 137.5°, PKP-Bdiff phase exhibits a very emergent onset, with a low amplitude and a large dominant period as compared to PKP_{DF} (PKIKP). It prevents an accurate estimation of the differential arrival times. Above 142.5°, the time separation between PKP-Bdiff and PKIKP is too small to avoid the possible contamination of PKIKP by PKP-Bdiff coda, due to the increasing amplitude of PKP-Bdiff at distances close to the caustic near 145°. Hence, here the PKIKP–PKP-Bdiff data lie in the distance range of 137.5°–142.5°.

The PKIKP–PKP-Cdiff data are recorded at epicentral distances between 154.4° and 162.6°, the range where PKP-Cdiff phase is generally observed. To improve the signal-to-noise ratio, a zero-phase low-pass Butterworth filter at 0.4 Hz has been applied to the PKIKP–PKP-Bdiff recordings to remove the short-period PKP precursors (Margerin and Nolet 2003). A similar filter at 1 Hz has been applied to the PKIKP–PKP-Cdiff observations, to increase their resemblance to the corresponding synthetics. An example of synthetic PKP phases is shown in Fig. 1.

For each event/station pair, we computed the synthetics corresponding to the hypocenter/station locations and Global Centroid Moment Tensor source

Table 1

The parameters of the events used in this study: normal font—the earthquakes which provided the PKP-Cdiff data; italic font—the earthquakes which provided PKP-Bdiff phases; bold font—the events which provided both B and Cdiff observations (according to the ISC Bulletin)

Region	Date	Origin time (UT)	Latitude	Longitude	Depth (km)	Mag
Fiji	1992-08-30	20:09:06.31	−17.9194	−178.7136	571.8	5.8
Vanuatu	1992-09-15	21:04:02.66	−14.1551	167.2552	211.5	6.3
S. Sandwich	1993-03-20	09:20:34.06	−56.0708	−27.8395	125.3	6.3
Honshu	1993-11-27	06:11:23.70	38.6074	141.2188	113.3	5.8
Vanuatu	1994-02-11	21:17:33.44	−18.81	169.1623	223.7	6.8
Fiji	1994-03-09	23:28:04.84	−17.9469	−178.4284	533.9	7.6
Vanuatu	*1994-05-04*	*06:37:37.88*	*−17.0950*	*168.2740*	*221.3*	*6.2*
S. Peru	1994-06-16	18:41:28.72	−15.3356	−70.2901	207.0	5.9
Banda	1994-07-13	11:45:22.39	−7.5034	127.8463	150.4	6.4
Argentina	1994-08-19	10:02:51.61	−26.6004	−63.3818	558.3	6.5
Java Sea	1994-09-28	17:34:00.24	−5.7677	110.5028	660.2	6.0
Java Sea	1994-11-15	20:18:11.46	−5.6177	110.2594	567.7	6.5
S. Kermadec	1994-12-27	17:32:51.86	−32.0525	179.8579	220.5	6.4
N. Peru	*1995-05-02*	*06:06:07.96*	*−3.7829*	*−76.9263*	*116.9*	*6.7*
New Britain	1995-08-14	04:37:21.38	−4.9024	151.4995	164.5	6.7
S.Fiji	1995-10-14	08:00:53.38	−25.7544	−177.5571	175.7	6.2
Kermadec	1997-04-12	09:21:47.33	−28.0954	−178.315	98.5	6.0
Santa Cruz	*1998-07-16*	*11:56:36.10*	*−11.0892*	*166.1731*	*109.5*	*7.0*
S.Fiji	2000-06-14	02:15:28.01	−25.6260	178.058	631.2	6.4
Chile-Argentina	2000-06-16	07:55:35.08	−33.811	−70.065	113.7	6.4
Kermadec	2000-08-15	04:30:08.23	−31.5610	179.7440	349.6	6.6
S.Fiji	2001-03-11	00:50:40.20	−25.540	−177.954	230.7	5.8
Fiji	**2001-04-28**	**04:49:51.92**	**−18.059**	**−176.937**	**340.6**	**6.8**
Fiji	**2001-05-19**	**17:36:26.60**	**−19.936**	**−177.492**	**374.7**	**5.9**
S.Bolivia	2001-06-29	18:35:50.94	−19.725	−66.272	271.9	6.1
Argentina	2002-09-24	03:57:20.90	−31.449	−69.139	104.6	6.2
W. Brazil	**2002-10-12**	**20:09:09.92**	**−8.3159**	**−71.6696**	**516.4**	**6.9**
Chile-Bolivia	2003-09-17	21:34:47.29	−21.427	−68.27	126.1	5.7
Argentina	*2005-03-21*	*12:23:53.07*	*−24.9411*	*−63.4567*	*576.6*	*6.8*
N.Peru	*2005-09-26*	*01:55:37.71*	*−5.7362*	*−76.4755*	*129.1*	*7.5*
Chile-Bolivia	2005-11-17	19:26:54.80	−22.2676	−67.9421	161.7	6.8
S. Fiji	2006-02-26	03:08:28.19	−23.6678	−179.9194	534.3	6.4
Fiji	2006-06-27	02:59:16.49	−19.9576	−178.230	574.9	6.3
Vanuatu	*2006-08-07*	*22:18:55.54*	*−15.8406*	*167.8174*	*148.5*	*6.8*
Chile-Argentina	2006-08-25	00:44:46.53	−24.345	−67.009	184.9	6.6
New Ireland	2007-04-21	07:12:48.32	−3.5537	151.3511	407.8	6.1
Fiji	2007-05-06	21:11:53.31	-19.4681	−179.3288	678.6	6.5
S. Fiji	2007-10-05	07:17:54.26	−25.1987	179.4462	521.3	6.5
Fiji	2007-11-19	00:52:12.51	−21.185	−178.752	558.3	6.3
Vanuatu	*2008-09-08*	*18:52:09.04*	*−13.5186*	*166.9846*	*124.7*	*6.9*
S. Bolivia	2008-10-12	20:55:41.91	−20.1808	−64.9821	357.8	6.2
Mindanao	2008-12-25	03:20:29.56	5.7760	125.5233	209.3	6.3
S. Honshu	2009-08-09	10:55:56.28	33.1474	138.0594	302.2	7.1
S.Fiji	2009-08-18	21:20:47.55	−26.064	−178.391	269.8	6.3
Kermadec	2009-09-02	18:00:09.33	−29.395	−178.956	257.0	6.2
Peru-Bolivia	2009-09-30	19:03:17.14	−15.6943	−69.4462	257.3	5.9
Fiji	2009-11-22	07:48:20.61	−17.794	−178.425	522.6	6.4
Kermadec	2009-11-22	22:47:27.48	−31.569	179.467	435.7	6.2
N.Chile	2010-03-04	22:39:25.71	−22.2651	−68.4579	108.4	6.3
New Ireland	2010-03-20	14:00:50.44	−3.3752	152.2786	418.9	6.6
W. Brazil	*2010-05-24*	*16:18:27.81*	*−8.1152*	*−71.6412*	*582.1*	*6.5*
S.Fiji	2010-06-30	04:31:02.16	−23.307	179.116	581.4	6.4
S. Sandwich	2011-03-06	14:32:36.94	−56.3864	−27.0253	92.0	6.5

Table 1 *continued*

Region	Date	Origin time (UT)	Latitude	Longitude	Depth (km)	Mag
Peru-Brazil	**2011-08-24**	**17:46:11.56**	**−7.6203**	**−74.538**	**149.3**	**7.0**
Banda Sea	*2011-08-30*	*06:57:41.54*	*−6.3592*	*126.7502*	*467.2*	*6.9*
Bolivia	2011-11-22	18:48:16.29	−15.3083	−65.1634	560.3	6.6
Fiji	2012-07-18	08:09:46.16	−20.8493	−178.4092	538.9	5.9
Vanuatu	*2012-12-21*	*22:28:08.08*	*−14.3591*	*167.2778*	*198.1*	*6.7*
Tonga	2013-05-11	20:46:57.50	−17.954	−175.099	212.2	6.4
S.Fiji	2014-03-26	03:29:35.72	−26.1147	179.264	497.8	6.4
S.Fiji	2014-05-04	09:15:52.88	−24.6108	179.0856	527.0	6.6
Fiji	2014-07-21	14:54:41.00	−19.8294	−178.464	616.4	6.9
N. Chile	2015-06-10	13:52:08.00	−22.4107	−68.3299	121.5	6.2
Vanuatu	**2015-10-20**	**21:52:02.00**	**−14.86**	**167.301**	**135.0**	**7.1**
Hindu-Kush	*2015-10-26*	*09:09:32.00*	*36.4406*	*70.7167*	*212.5*	*7.5*
Peru-Brazil	*2015-11-24*	*22:45:38.00*	*−10.55*	*−70.90*	*600.6*	*7.6*
Peru-Brazil	**2015-11-26**	**05:45:18.00**	**−9.19**	**−71.29**	**599.4**	**6.7**

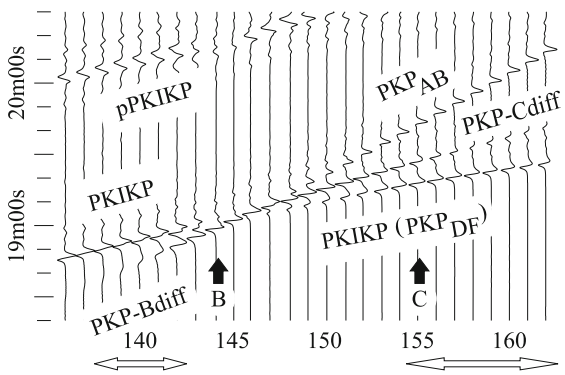

Figure 1
Travel time vs epicentral distance for the main core phases in the distance range of 136°–162°. Synthetic waveforms obtained by normal modes summation correspond to a point source at 300 km depth, and ak135 global model. The positions of the B (caustic point) and C (cut off point) are indicated. Each trace is scaled to a common value of the maximum amplitude. The amplitude of PKiKP (the core phase reflected from the ICB) is very small, if any. That phase should follow PKIKP by 1.7 s at 136° and by 3.6 s at 144°. At 150°, PKiKP follows PKP_{BC} by approximately 0.8 s and this time separation vanishes at the C—cut off point (near 155°). The *two horizontal arrows* show the range of the epicentral distances used in this analysis (namely, from 137.5° to 142.5° for Bdiff, respectively, from 154.4° to 162.6° for Cdiff)

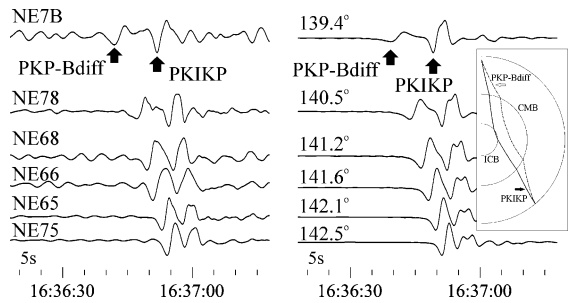

Figure 2
PKP-Bdiff observations (vertical channel) of 2010, May 24th event of Western Brazilia, at several temporary stations of the North-East China extended seismic array (*left*), and the corresponding synthetics (*right*). The raw broad-band velocity data (and synthetics) have been filtered with a zero-phase low-pass Butterworth filter at 0.4 Hz. The *inset* shows the ray path of PKIKP and the approximate path PKP-Bdiff phases at the distance of ∼140°

parameters (Dziewonski et al. 1981; Ekström et al. 2012) using the normal modes theory (Wang 1999) and ak135 global model. The earthquake catalog is from the reviewed ISC Bulletin (Engdahl and Gunst 1966). Examples of recorded and synthetic diffracted core phases are displayed in Figs. 2 and 3.

The observed core phases exhibit a high similarity compared to the synthetics, ensuring the calculation of the differential PKIKP–PKP-Bdiff and PKIKP–PKP-Cdiff travel times using the waveform cross-correlation of time windows consisting, routinely, of the first semi-cycle of each phase (e.g., Irving and Deuss 2011; Tanaka 2012). The differential time residuals are presented in Fig. 4 for PKIKP–PKP-Bdiff and in Fig. 5 for PKIKP–PKP-Cdiff, along the ray path of PKIKP into the IC, respectively. Assuming that the residual values are mainly related to IC, we evaluate the average P-wave velocity perturbations with respect to the reference model $\Delta v/v$ in the IC using the first-order approximation (applicable when $\Delta v/v \ll 1$)

$$\Delta v/v = -\Delta t/t_{IC}, \quad (1)$$

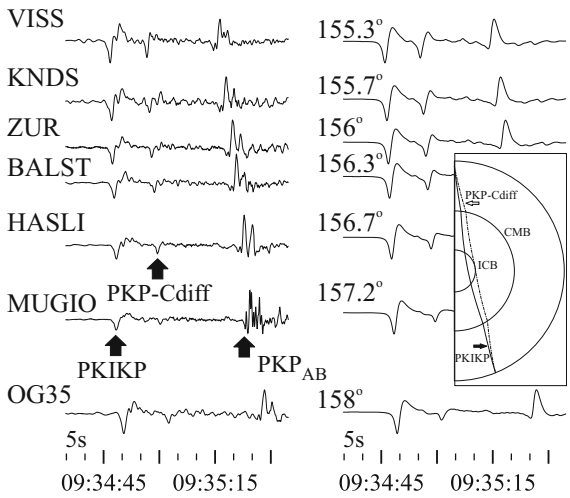

Figure 3
PKP-Cdiff observations (vertical channel) of 2014, May 4th event of Fiji, at several European stations (*left*), and the corresponding synthetics (*right*). The raw broad-band velocity data have been filtered with a zero-phase low-pass Butterworth filter at 1 Hz. The *inset* shows the ray paths of PKIKP and PKP-Cdiff phases at the distance of 158°. The diffraction path along ICB is around 3° here

where Δt is the differential travel-time residual and t_{IC} is the travel time of PKIKP in the IC. Adopting the geographic definition for the IC quasi-hemispheres (i.e., the QEH between 0° and 180°E, and the QWH between 0° and 180°W), we selected 850 PKIKP–PKP-Cdiff and 229 PKIKP–PKP-Bdiff residual data in the QEH, respectively, 258 PKIKP–PKP-Cdiff and 171 PKIKP–PKP-Bdiff residual data in the QWH, performing a basic statistical analysis of the estimated average $\Delta v/v$ values. The obtained velocity perturbation histograms (Fig. 6) show normal distributions, except the one corresponding to PKP-Cdiff in QWH, which likely points to a bimodal distribution. This is mainly the result of the positive differential time residuals obtained at Japanese F-Net stations for two events sourced from Chile and Argentina (occurred on 2000, June 16th and 2002, September 24th), and at several Chilean stations for the Southern Honshu event on 2009, August, 9th.

The average P-wave velocity perturbation with respect to ak135, estimated from the PKIKP–PKP-Bdiff recordings—with the PKIKP rays bottoming in the approximate depth range of 50–100 km beneath the ICB—is $(+1.17 \pm 0.04)$ % in the QEH (from 229 observations) and (-0.06 ± 0.06) % in the QWH (from 171 values). Likewise, the average P-wave velocity perturbation determined from the PKIKP–PKP-Cdiff data–PKIKP bottoming roughly

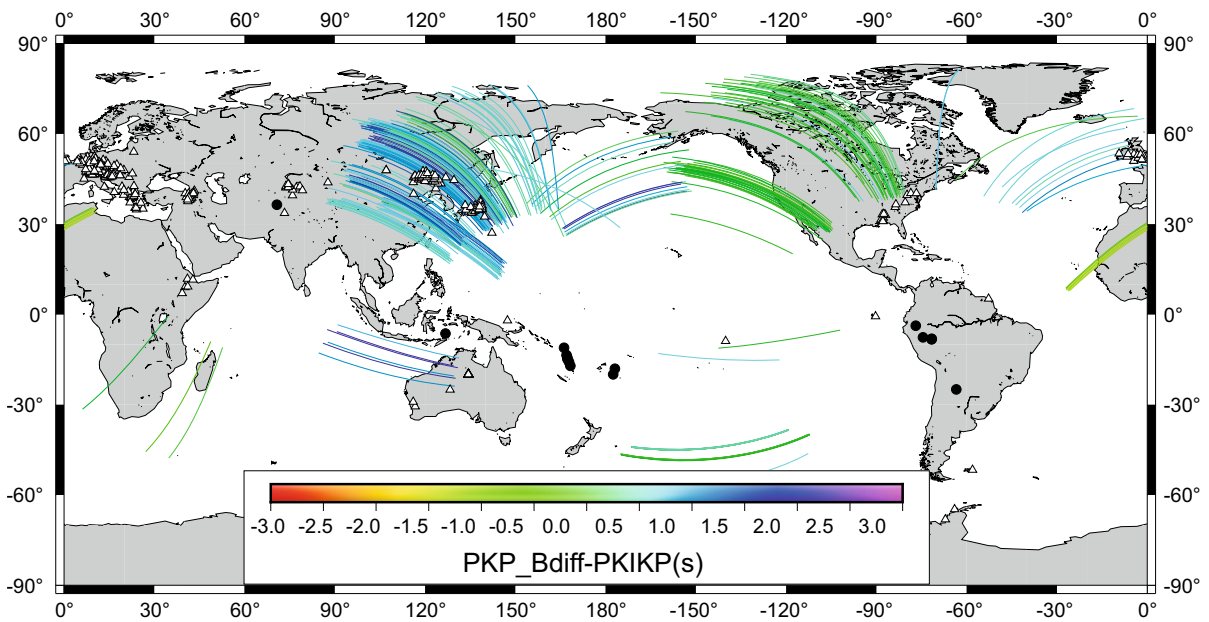

Figure 4
The O-C differential travel times for PKP–Bdiff vs. PKIKP

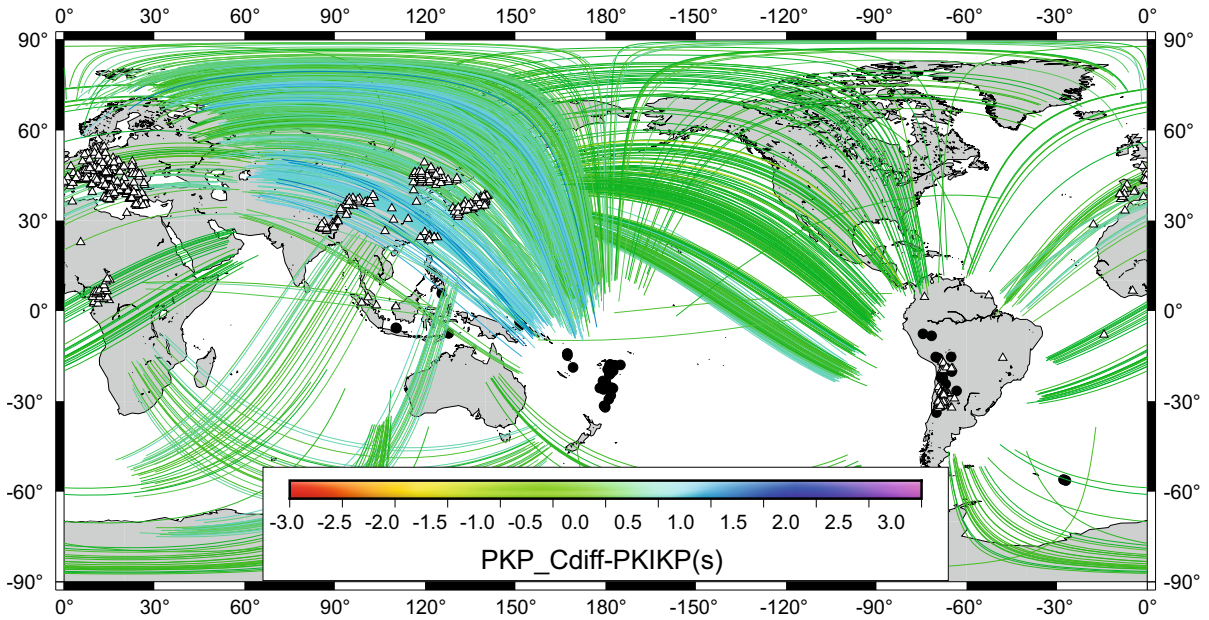

Figure 5
The O-C differential travel times for PKP-Cdiff vs. PKIKP

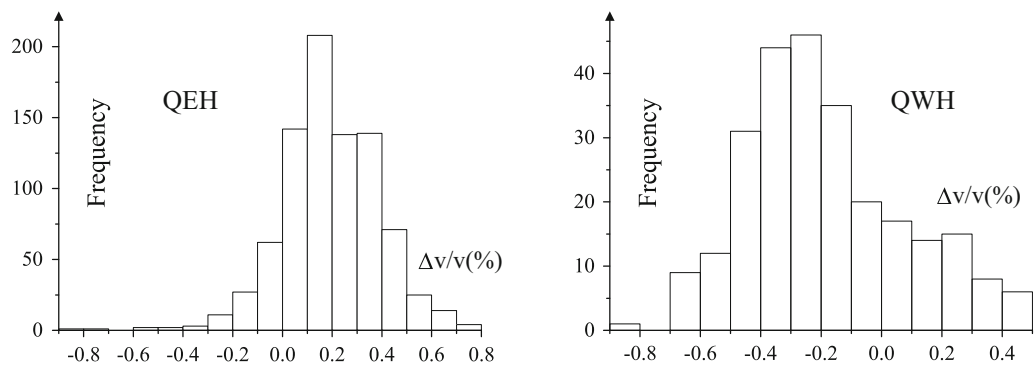

Figure 6
Histograms of the P-wave velocity perturbations with respect to ak135 model in the IC, obtained from PKP-Cdiff vs PKIKP observations for the QEH (*left*) and QWH (*right*). A bimodal distribution is suggested for the QWH, with a second maximum near 0.2 %, consistent with QEH distribution

in the depth range of 350–590 km beneath the ICB—is $(+0.19 \pm 0.01)$ % in the QEH (from 850 values) and (-0.19 ± 0.02) % in the QWH (from 258 observations).

3. *Discussion and Conclusions*

In general, the differential travel-time residuals of the core phases are considered to be related to the heterogeneity/anisotropy in the IC. However, there is a bias mainly related to the heterogeneities in the D" layer, especially for the phase pairs with a larger separation of their core–mantle boundary piercing points. Regarding PKP-Bdiff vs. PKIKP, the corresponding separation (around 16°) is less than the one for PKP_{AB} (P wave bottoming in the upper OC) vs. PKIKP (which exceeds 25°), but greater than the one for PKP_{BC} vs. PKIKP (which is around 4.5°. Although PKP-Bdiff phase is not predicted by ray

theory in relation to standard global models (e.g., TauP Toolkit, Crotwell et al. 1999; 'ttimes' software, Kennett et al. 1995), it can be quite accurately synthesized by modal summation to 1 Hz, with an apparent slowness of about 3.8 s/°. Thus, PKP-Bdiff is apparently bottoming around 850 km above ICB and its propagation time is virtually independent of velocity disturbances in LOC. Luo et al. (2002) suggested that the situations are statistically rare where most of the relatively long-period Bdiff leg in the proximity of the CMB will be in a low or ultra-low-velocity zone (ULVZ). We further investigate the effect of an ULVZ with a −15 % P-wave velocity perturbation on the synthetic seismograms. The differential times PKIKP–PKP-Bdiff evaluated for the seismograms computed with ak135 model incorporating an ULVZ are reduced in respect to the values obtained with the ak135 model from 1.5 s (at 139° distance) to 1 s at 140.8°, with a clear slowness change around 0.3 s/°. In real observations, we see no clear trend in the (O-C) differential times PKIKP–PKP-Bdiff, if the computations are done with ak135 model (Fig. 7). In detail, for the Vanuatu events recorded at a large number of European stations, we obtain no statistically reliable difference between the slowness of the observed PKP-Bdiff and the same value of the corresponding synthetics. We conclude that in our global study, velocity heterogeneities in D" are expected to have a small effect on the differential times related to PKP-Bdiff, in agreement to Luo et al. (2002). The crust and mantle contribution to PKP-Bdiff vs. PKIKP differential times is further investigated using the 3-D LLNL global model of Simmons et al. (2012). The values show almost no geographical variations, but they slightly emphasize the hemispherical pattern observed in the recordings (Fig. 8).

The PKP-Cdiff and PKIKP phases show a smaller separation of their piercing points to core–mantle boundary (around 4.2°), by comparison to other phase pairs (e.g.,PKP_{BC} vs. PKIKP or PKP_{AB} vs. PKIKP). Consequently, their differential travel times are the least sensitive to the heterogeneities from the source region and from the mantle along the ray path (especially in D" layer). In fact, the crust/mantle contribution to PKP-Cdiff vs. PKIKP differential times evaluated with the LLNL 3-D model shows

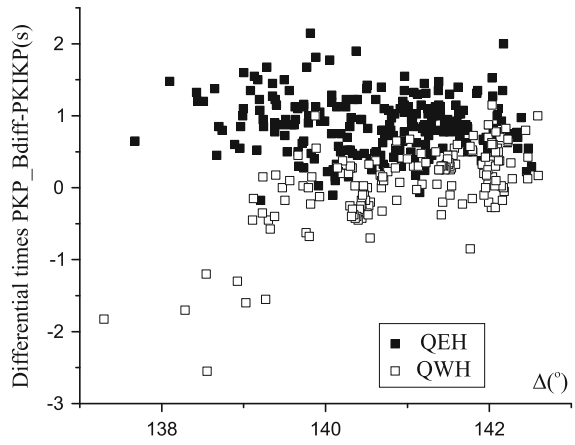

Figure 7
The differential times PKB-Bdiff vs PKIKP as a function of the epicentral distance

small values around −0.2 s with no significant geographical variation. Thus, the crust/mantle on the PKP-Cdiff vs. PKIKP differential times is negligible (Fig. 9). However, PKIKP vs. PKP-Cdiff differential travel-time residuals can be alternatively interpreted as a result of velocity perturbations at the base of the outer core (Yu et al. 2005). This is the case especially when large anomalous amplitude ratio values, or significant trailing coda of PKP-Cdiff are observed (Zou et al. 2008). Our observations do not exhibit such features, in general. The travel time of PKP-Cdiff along the ICB (length of diffracted path around 5°) is close to 10 s for a ray parameter around 2 s/°. Consequently, realistic variations of P-wave velocity in the lowermost OC (around 2–3 %) would result in variations of the PKP-Cdiff travel time around 0.2–0.3 s, significantly smaller than our observed residuals (Fig. 10). When compared to the corresponding ak135 synthetics, the differential times PKIKP vs. PKP-Cdiff show no statistically reliable trend with respect to the epicentral distance (Fig. 11). Again, we conclude that the velocity heterogeneities on F layer are expected to have a small effect in our global investigation, but we cannot exclude that, and it could be of interest in some other restricted areas, not covered by our study.

The reference models used in synthetic computations also bias the differential arrival times of the core phases. In this study, the synthetic seismograms show that the ak135 model can be legitimately used

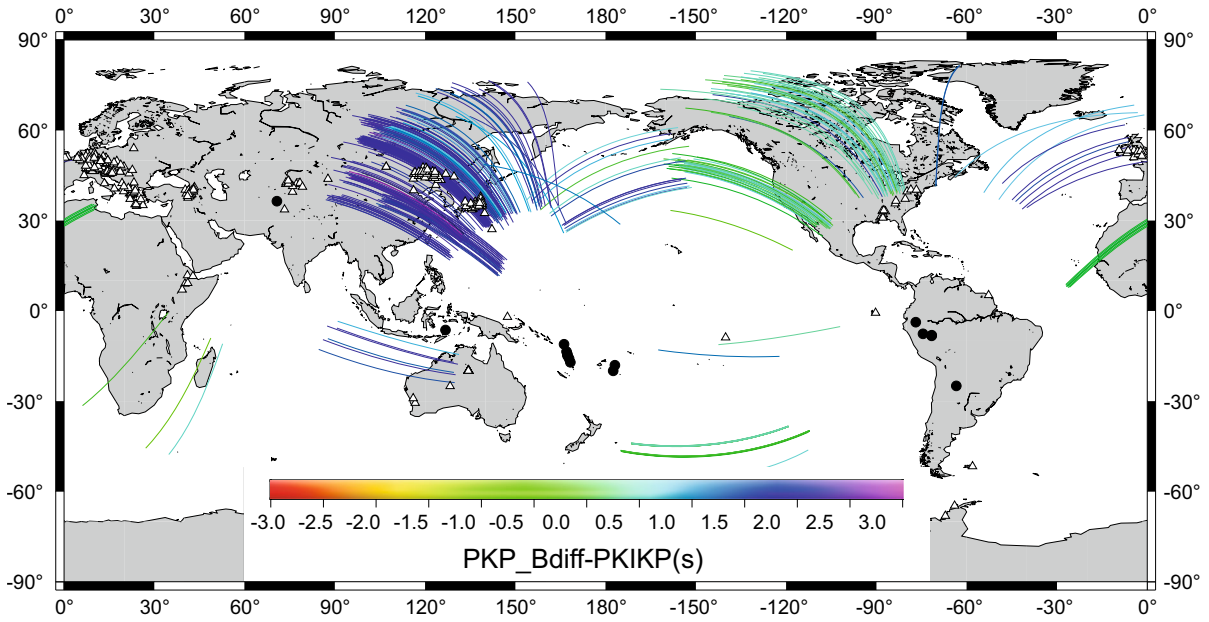

Figure 8
The PKB-Bdiff vs PKIKP differential times corrected for the effect of crust/mantle heterogeneities evaluated with LLNL 3D global model (Simmons et al. 2012)

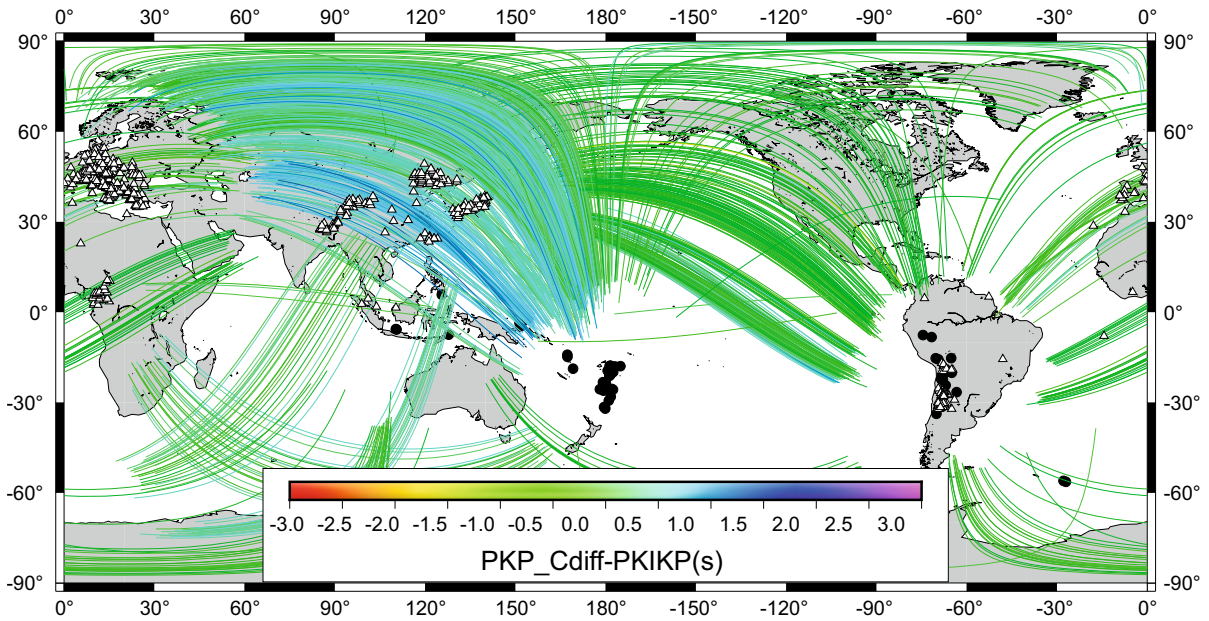

Figure 9
The same caption as Fig. 8, but for PKP-Cdiff

as a global reference model, with no need to significantly change the parameters of the global model in D" or in the F layer.

Our main dataset samples the IC well along the equatorial path, but there are no pole-parallel paths (Figs. 12, 13). Most of the cases displaying strong

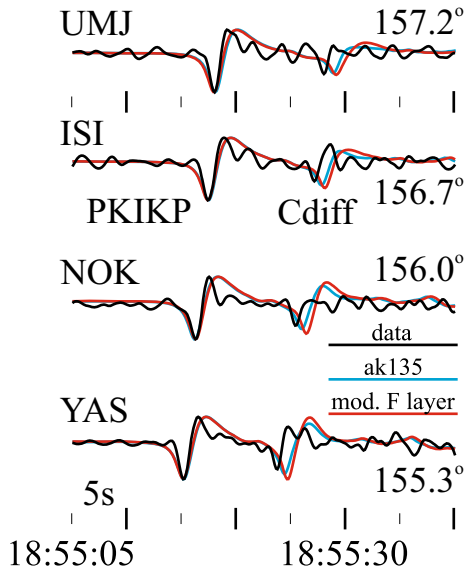

Figure 10
Recordings at some Japanese stations of 2001, June 29th South Bolivia event. The synthetics are evaluated with ak135 model (*blue*). *Red traces* are the synthetics obtained by modifying the F layer similar to Ohtaki and Kaneshima (2015). Traces are aligned to PKIKP arrival times

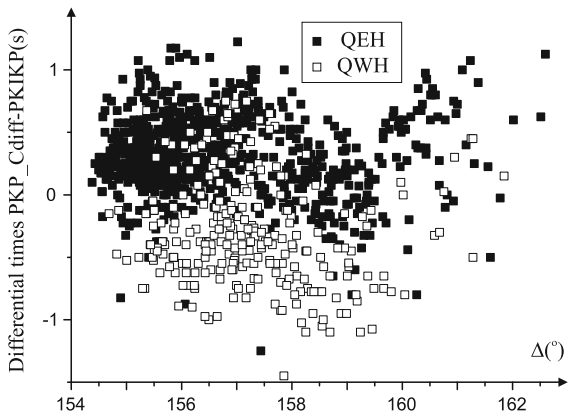

Figure 11
The differential times PKB-Cdiff vs PKIKP as a function of the epicentral distance

anisotropy in the IC have been observed for nearly pole-parallel paths. Consequently, we are not able to discuss further the IC anisotropy, but the hemispherical differences we observe do suggest heterogeneity of some kind.

Considering the routine separation between the IC quasi-hemispheres along the 180°W meridian, for the QEH we found a positive average velocity

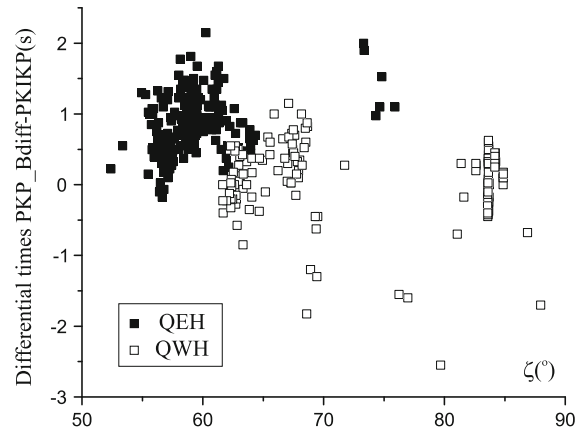

Figure 12
The differential times PKB-Bdiff vs PKIKP as a function of the angle between the PKIKP inner core path and the Earth's spin axis

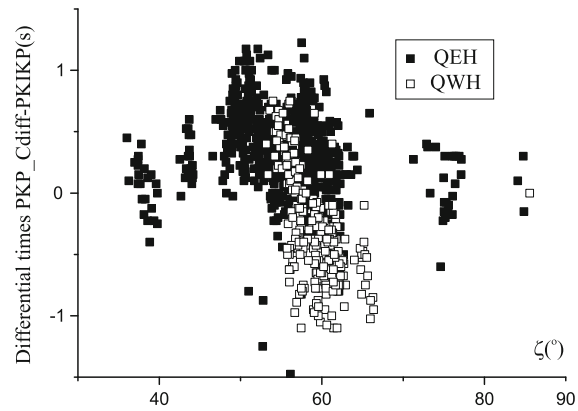

Figure 13
The differential times PKB-Cdiff vs PKIKP as a function of the angle between the PKIKP inner core path and the Earth's spin axis

perturbation with respect to the reference model, varying from (+1.17 ± 0.04) % at the top of ICB to (+0.19 ± 0.01) % at depth in the range of 350–590 km beneath ICB, well correlated with the observations on wave attenuation reported by Iritani et al. (2014). Beneath the Pacific, the separation between the observed positive and negative velocity perturbations appears to be along 150°W meridian line from PKP-Bdiff differential times (i.e., at the top of the IC), a longitude value close to Irving and Deuss (2011). However, PKP-Cdiff observations suggest the boundary between QEH and QWH to be apparently rotated to a North–West–South–East direction and a smooth transition between them. Such a possibility is

also supported by the PKP_{BC}–PKIKP results in the same area of Yee et al. (2014). It could be a result of melting and crystallizing poles axis (Monnereau et al. 2010) deviating from the Earth's equatorial plane. An alternate explication could be an anomalous LOC here, as suggested by Ohtaki and Kaneshima (2015), or velocity variations in the IC. In conclusion, the velocity perturbations in the UIC seem to be more intricate than suggested by a simple quasi-hemispheric pattern (along a longitude line), in agreement, e.g., to Ohtaki et al. (2012), to Iritani et al. (2014) or to Krasnoshchekov et al. (2016).

The separation between the IC quasi-hemispheres beneath North Atlantic appears to be between 60°W and 30°W from the PKP-Bdiff observations, but it remains unresolved from the PKP-Cdiff data due to a small number of data here.

The number of observations related to the Earth's Southern hemisphere is less abundant. For the Pacific Ocean, PKP-Bdiff observations predict a similar IC hemispheric separation also around 150°W, but the separation remains again unresolved from the PKP-Cdiff observations. While several authors reported an anomalous IC zone beneath the Indian Ocean (e.g., Monnereau et al. 2010; Cormier and Attanayake 2013), this is not conspicuous in our observations, i.e., in the depth range of 350–590 km beneath the ICB.

Despite the fact that the LLNL 3-D global model cannot be directly linked to ak135, the evaluation of crust and mantle heterogeneities effect on the differential travel times of the diffracted core phases suggests that the difference between the velocity perturbations in the two IC quasi-hemispheres are slightly greater than our estimations for the top of the inner core (Fig. 8). By contrast, they remain unchanged for the deeper IC (Fig. 9). Future 3-D velocity global models defined in a reference to ak135 are of assistance in accurate evaluation of the velocity perturbations inside the inner core.

Acknowledgments

Data to support this article are freely available at IRIS, ORFEUS and F-Net data centers. We thank R. Wang for providing the QSSP code used to compute the synthetics and N. A. Simmons for detailed discussions on LLNL 3-D global model. X. H. was supported by the National Science Foundation of China (Grant 41330207).

References

Alboussière, T., Deguen, R., & Melzani, M. (2010). Melting-induced stratification above the Earth's inner core due to convective translation. *Nature, 466*, 744–747.

Cormier, V. F., & Attanayake, J. (2013). Earth's solid inner core: Seismic implications of freezing and melting. *Journal of Earth Science, 24*, 683–698. doi:10.1007/s12583-013-0363-9.

Creager, K. C. (1999). Large-scale variations in inner core anisotropy. *Journal Geophysical Research, 104*, 23127–23139.

Crotwell, H. P., Owens, T. J., & Ritsema, J. (1999). The TauP toolkit: Flexible seismic travel-time and ray-path utilities. *Seismological Research Letters, 70*, 154–160.

Deuss, A. (2014). Heterogeneity and anisotropy of earth's inner core. *Annual Review of Earth and Planetary Sciences, 42*, 103–126. doi:10.1146/annurev-earth-060313-054658.

Deuss, A., Irving, J. C. E., & Woodhouse, J. H. (2010). Regional variation of inner core anisotropy from seismic normal mode observations. *Science, 328*, 1018–1020.

Dziewonski, A. M., Chou, T.-A., & Woodhouse, J. H. (1981). Determination of earthquake source parameters from waveform data for studies of global and regional seismicity. *Journal Geophysical Research, 86*, 2825–2852. doi:10.1029/JB086iB04p02825.

Ekström, G., Nettles, M., & Dziewonski, A. M. (2012). The global CMT project 2004–2010: Centroid-moment tensors for 13,017 earthquakes. *Physics of the Earth and Planetary Interiors, 200–201*, 1–9. doi:10.1016/j.pepi.2012.04.002.

Engdahl, E. R., & Gunst, R. H. (1966). Use of a high speed computer for the preliminary determination of earthquake hypocenters. *Bulletin of the Seismological Society of America, 56*, 325–336.

International Seismological Centre. *On-line Bulletin.* http://www.isc.ac.uk. Thatcham: International Seismological Centre (2013).

Iritani, R., Takeuchi, N., & Kawakatsu, H. (2014). Intricate heterogeneous structures of the top 300 km of the Earth's inner core inferred from global array data: I. Regional 1D attenuation and velocity profiles. *Physics of the Earth and Planetary Interiors, 230*, 15–27.

Irving, J. C. E., & Deuss, A. (2011). Hemispherical structure in inner core velocity anisotropy. *Journal Geophysical Research, 116*, B04307.

Kennett, B. L. N., Engdahl, E. R., & Buland, R. (1995). Constraints on seismic velocities in the Earth from traveltimes. *Geophysical Journal International, 122*, 108–124.

Krasnoshchekov, D., Kaazik, P., Kozlovskaya, E., & Ovtchinnikov, V. (2016). Seismic structures in the Earth's inner core below Southeastern Asia. *Pure and Applied Geophysics, 173*, 1575–1591.

Krasnoshchekov, D. N., Kaazik, P. B., & Ovtchinnikov, V. M. (2005). Seismological evidence for mosaic structure of the surface of the Earth's inner core. *Nature, 435*, 483–487.

Loper, D. E., & Roberts, P. H. (1981). A study of conditions at the inner core boundary of the Earth. *Physics of the Earth and Planetary Interiors, 24*, 302–307.

Luo, S.-N., Ni, S., & Helmberger, D. (2002). Relationship of D" structure with the velocity variations near the inner-core boundary. *Geophysical Reseach Letters*. doi:10.1029/2001GL013907.

Margerin, L., & Nolet, G. (2003). Multiple scattering of high-frequency seismic waves in the deep Earth: PKP precursor analysis and inversion for mantle granularity. *Journal Geophysical Research, 108*(B11), 2514. doi:10.1029/2003JB002455.

Monnereau, M., Calvet, M., Margerin, M., & Souriau, A. (2010). Lopsided growth of Earth's inner core. *Science, 328*, 1014–1017.

Niu, F., & Wen, L. (2001). Hemispherical variations in seismic velocity at the top of the Earth's inner core. *Nature, 410*, 1081–1084.

Ohtaki, T., & Kaneshima, S. (2015). Independent estimate of velocity structure of Earth's lowermost outer core beneath the northeast Pacific from PKiKP-PKPbc differential traveltime and dispersion in PKPbc. *Journal of Geophysical Research: Solid Earth*, *120*. doi:10.1002/2015JB012140

Ohtaki, T., Kaneshima, S., & Kanjo, K. (2012). Seismic structure near the inner core boundary in the South Polar Region. *Journal of Geophysical Research*, *117*, B03312. doi:10.1029/2011JB008717.

Simmons, N. A., Myers, S. C., Johannesson, G., & Matzel, E. (2012). LLNL-G3Dv3: Global P wave tomography model for improved regional and teleseismic travel time prediction. *Journal Geophysical Research, 117*, B10302. doi:10.1029/2012JB009525.

Souriau, A., Garcia, R., & Poupinet, G. (2003). The seismological picture of the inner core: structure and rotation. *Comptes Rendus Geoscience, 335*, 51–63.

Sun, X., & Song, X. (2002). PKP traveltimes at near antipodal distances: Implications for inner core anisotropy and lowermost mantle structure. *Earth and Planetary Science Letters*, *199*, 429–445.

Tanaka, S. (2012). Depth extent of hemispherical inner core from PKP(DF) and PKP(Cdiff) for equatorial paths. *Physics of the Earth and Planetary Interiors, 210–211*, 50–62.

Tanaka, S., & Hamaguchi, H. (1997). Degree one heterogeneity and hemispherical variation of anisotropy in the inner core from PKP (BC)–PKP (DF) times. *Journal Geophysical Research, 102*, 2925–2938.

Tkalcic, H. (2015). Complex inner core of the Earth: The last frontier of global seismology. *Reviews of Geophysics 53*, 59–94. doi:10.1002/2014RG000469.

Wang, R. (1999). A simple orthonormalization method for the stable and efficient computation of Green's functions. *Bulletin of the Seismological Society of America, 89*, 733–741.

Wen, L., & Helmberger, D. V. (1998). Ultra-low velocity zones near the core-mantle boundary from broadband PKP precursors. *Science, 279*, 1701–1703.

Yee, T.-G., Rhie, J., & Tkalčić, H. (2014). Regionally heterogeneous uppermost inner core observed with Hi-net array. *Journal Geophysical Research*. doi:10.1002/2014JB011341.

Yu, W., & Wen, L. (2006). Seismic velocity and attenuation structures in the top 400 km of the Earth's inner core along equatorial paths. *Journal Geophysical Research, 111*, B07308. doi:10.1029/2005JB003995.

Yu, W., Wen, L., & Niu, F. (2005). Seismic velocity structure in the Earth's outer core. *Journal Geophysical Research, 110*, B02302. doi:10.1029/2003JB002928.

Zou, Z., Koper, K. D., & Cormier, V. F. (2008). The structure of the base of the outer core inferred from seismic waves diffracted around the inner core. *Journal Geophysical Research, 113*, B05314. doi:10.1029/2007JB005316.

(Received March 25, 2016, revised July 18, 2016, accepted August 30, 2016)